



**HAL**  
open science

## Coupled effects of Mn(ii), pH and anionic ligands on the reactivity of nanostructured birnessite

Qinzhi Li, Rasesh Pokharel, Lian Zhou, Mathieu Pasturel, Khalil Hanna

### ► To cite this version:

Qinzhi Li, Rasesh Pokharel, Lian Zhou, Mathieu Pasturel, Khalil Hanna. Coupled effects of Mn(ii), pH and anionic ligands on the reactivity of nanostructured birnessite. *Environmental science.Nano*, 2020, 7 (12), pp.4022-4031. 10.1039/d0en01046d . hal-03122466

**HAL Id: hal-03122466**

**<https://hal.science/hal-03122466>**

Submitted on 16 Feb 2021

**HAL** is a multi-disciplinary open access archive for the deposit and dissemination of scientific research documents, whether they are published or not. The documents may come from teaching and research institutions in France or abroad, or from public or private research centers.

L'archive ouverte pluridisciplinaire **HAL**, est destinée au dépôt et à la diffusion de documents scientifiques de niveau recherche, publiés ou non, émanant des établissements d'enseignement et de recherche français ou étrangers, des laboratoires publics ou privés.

1 **Coupled effects of Mn(II), pH and anionic ligands on the reactivity**  
2 **of nanostructured birnessite**

3  
4  
5  
6 Qinzhi Li<sup>a</sup>, Rasesh Pokharel<sup>a</sup>, Lian Zhou<sup>a</sup>, Mathieu Pasturel<sup>b</sup>, Khalil Hanna<sup>a,c,\*</sup>

7  
8 <sup>a</sup>*Univ. Rennes, École Nationale Supérieure de Chimie de Rennes, CNRS, ISCR – UMR6226, F-*  
9 *35000 Rennes, France*

10 <sup>b</sup> *Univ. Rennes, CNRS, ISCR – UMR 6226, F-35000, Rennes, France*

11 <sup>c</sup>*Institut Universitaire de France (IUF), MESRI, 1 rue Descartes, 75231 Paris, France.*

12  
13  
14  
15  
16 \*Corresponding author: K Hanna, 0033 2 23 23 80 27; [khalil.hanna@ensc-rennes.fr](mailto:khalil.hanna@ensc-rennes.fr)

21 **Abstract**

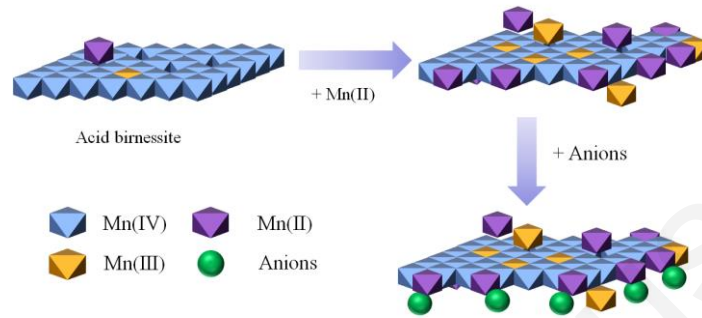
22 While the oxidative capacity of nanostructured birnessite-type manganese oxide has been  
23 widely investigated, no comprehensive work exists on the combined effects of dissolved Mn(II),  
24 pH and inorganic anions on sorption and redox reactions of organic contaminants with MnO<sub>2</sub>.  
25 Herein, we have showed how molecular interactions of two contrasting organic contaminants,  
26 Pipemidic acid (PIP) and Bisphenol A (BPA), with MnO<sub>2</sub> surfaces controlled on the removal  
27 kinetic behavior, which depended on contaminant type and co-existing anions. Competition  
28 between contaminant and Mn(II) for binding at the edge sites determined the initial kinetic step,  
29 while buildup of Mn(II) at both edge and vacancy sites continuously decreased adsorption and  
30 subsequent oxidation over time. Redox interactions of Mn(II) to MnO<sub>2</sub> surfaces was a pH  
31 dependent process, and high pH favored Mn(II) removal and comproportionation reaction, thus  
32 decreasing adsorption and oxidation processes. At low Mn(II)/MnO<sub>2</sub> ratio, MnO<sub>2</sub> adsorbed more  
33 effectively anions such as phosphate or silicate, thus reducing interactions with organic  
34 compounds. These results highlight the combined suppressive effects of Mn(II), pH and naturally  
35 occurring anions on the reactivity of nanostructured birnessite, and have strong implications on the  
36 fate of organic contaminants in terrestrial and aquatic environments.

37 **Keywords:** nanostructured birnessite; redox; emerging contaminants; adsorption; oxidation.

38

### Table of contents

39 Dissolved Mn(II), pH and naturally occurring anions exhibit combined suppressive effects on the  
40 reactivity of nanostructured birnessite.



41

42

## 43 1. Introduction

44 Manganese oxide / hydroxide (referred here as Mn oxide) are ubiquitous in a wide range of  
45 environmental settings, such as soils, sediments, rock dendrites, desert varnishes, ocean floor, and  
46 fresh-water bodies.<sup>1, 2</sup> Because they are powerful oxidants and sorbents, they play a key role in the  
47 biogeochemical cycle of many elements.<sup>1</sup> Based on the mineral structure, manganese oxides can  
48 be divided into two types: layer and tunnel structure.<sup>1</sup> Layered structure manganese oxides (e.g.  
49 birnessite) has gathered interest because it is structurally similar to biogenically precipitated natural  
50 manganese oxides.<sup>3-6</sup> The structure of layered birnessite consists of mineral sheets of hexagonal  
51 symmetry comprising of edge-sharing  $MnO_6$  octahedra, accompanied by interlayer charge-  
52 neutralizing cations.<sup>3, 7-10</sup> Because of the existence of Mn(III) and possibly Mn(II) within the  $MnO_2$   
53 layers, it has a manganese average oxidation state (AOS) lower than 4.<sup>11</sup> Typically, birnessite have  
54 high affinity for cations sorption because of high content of vacancy sites, with up to one out of six  
55 Mn absent from  $MnO_6$  octahedral sites,<sup>12, 13</sup> but they also exhibit non-negligible anion adsorption  
56 capacity.<sup>14-18</sup> Another important feature of birnessite is the easy switching of the oxidation state,  
57 which imparts a good catalytic activity.<sup>10, 19</sup> Therefore, nanostructured birnessite-type manganese  
58 oxides take part in redox-based and cation-exchange reactions with potential for various energy  
59 and environmental applications.<sup>1, 20-25</sup>

60 Generally, binding of redox-active compounds to birnessite is followed by an electron  
61 transfer process resulting in the concomitant oxidation of sorbed compound and reduction of  
62 surface-bound metal. Typically, one electron is transferred from ligand to the surface-bound Mn(IV)  
63 to yield Mn(III) that can be further reduced to give Mn(II).<sup>17, 23, 24, 26, 27</sup> This reactivity is mainly  
64 affected by solution pH, oxide surface properties, and structural characteristics of target  
65 compound.<sup>23, 24, 28-30</sup> Some studies have shown that the presence of dissolved Mn(II) induces

66 changes in mineral structure and reactivity of MnO<sub>2</sub>, but this effect depends on the Mn(II)/MnO<sub>2</sub>  
67 ratio and pH value. A high Mn(II)/MnO<sub>2</sub> ratio and pH > 7.5, birnessite can be converted into lower-  
68 valence Mn phases, while only slight disturbance in the stacking of MnO<sub>2</sub> sheets caused by  
69 incorporation of Mn(III) can be observed at low Mn(II)/MnO<sub>2</sub> ratio and at acidic to neutral pH.<sup>31</sup>  
70 <sup>32</sup> Although the effects of dissolved Mn(II) on the structure and AOS of birnessite have been well  
71 investigated,<sup>5, 17,31-34</sup> knowledge is limited on how co-existing anions and dissolved Mn(II) affect  
72 the dynamic changes of birnessite reactivity towards adsorption and oxidation of organic  
73 compounds. In addition, surface interactions of organic ligands with MnO<sub>2</sub> in the presence of  
74 dissolved Mn(II) and naturally occurring anions during birnessite partial reduction under a wide  
75 range of pH have been scarcely investigated.

76 In this study, we examined how dissolved Mn(II), which is commonly found in  
77 groundwater from  $\mu\text{M}$  to mM concentration ranges<sup>35,36</sup> affects the interactions of organic  
78 compounds with MnO<sub>2</sub> surfaces and the reactivity of birnessite under different experimental  
79 conditions. For this purpose, two contrasting organic contaminants, Pipemidic acid (PIP) and  
80 Bisphenol A (BPA), frequently detected in aquatic environments such as surface water and  
81 groundwater<sup>37-39</sup> were selected as environmentally relevant model compounds. PIP is a synthetic  
82 broad-spectrum antibacterial belonging to quinolone antibiotics, and widely used to treat various  
83 infections in human and veterinary medicine.<sup>25</sup> Quinolones are electron donor-acceptor  
84 compounds with the piperazinyl group serving as the electron donor and carboxylic group as the  
85 electron acceptor in the neutral and zwitterion forms.<sup>27, 40</sup> Bisphenol A is an important endocrine-  
86 disrupting compound, and contains two hydroxyphenyl functionalities. Nanoflower-shaped  
87 birnessite, a poorly crystalline Mn oxide and ubiquitous in nature, was chosen as a representative  
88 manganese oxide mineral. The surface interactions of PIP or BPA including adsorption and

89 oxidation with birnessite have been investigated in presence of variable amounts of Mn(II) and  
90 under a wide range of pH (4-8). Total removal rates including the rate-determining step have been  
91 determined using different kinetic models. The oxidation byproducts of BPA and PIP were  
92 identified using Ultrapformance Liquid Chromatography-tandem Mass Spectrometry (UPLC-  
93 MS/MS) system. The impact of Mn(II) was also studied in presence of commonly found natural  
94 anions, phosphate and silicate. The possible transformation of solid has been monitored using XRD  
95 and ATR-FTIR under different conditions (Mn(II)/MnO<sub>2</sub> ratio and pH value). Finally, the  
96 reactivity changes of birnessite due to the combined effects of Mn(II), pH and anionic ligands and  
97 underlying mechanisms were discussed.

## 98 **2. Materials and Methods**

### 99 2.1. Materials

100 All reagents were purchased from Sigma-Aldrich and used without further purification. All  
101 solutions were prepared with ultrapure water (specific resistivity, 18.2 MΩ cm<sup>-1</sup>, Milli-Q,  
102 Millipore).

### 103 2.2. Acid birnessite synthesis and characterization

104 Acid birnessite was prepared following the procedures of McKenzie.<sup>41</sup> 166 mL of  
105 concentrated HCl was added dropwise to 2.5 L of 0.4 M KMnO<sub>4</sub>. The suspension was stirred  
106 vigorously and kept at 90°C during the HCl addition. The reaction was continued at 90 °C for a  
107 further 10 min. Then, the obtained slurry was stirred vigorously at room temperature for 15 h. The  
108 precipitate was collected by centrifugation, washed with ultrapure water repeatedly until the  
109 conductivity was close to 0.6 μS cm<sup>-1</sup>. The suspensions were stored in polypropylene containers at  
110 4 °C for further use.

111 The purity of acid birnessite was confirmed by powder X-ray diffraction (XRD) (Figure  
112 S1). The XRD data were recorded with the monochromatized CuK $\alpha$  radiation on a Bruker AXS  
113 D8 Advance diffractometer ( $\theta$ -2 $\theta$  Bragg-Brentano geometry) over the range of 10 $^\circ$ -100 $^\circ$  2 $\theta$  at a  
114 step size of 0.02 $^\circ$ . The N $_2$  Brunauer–Emmett–Teller (BET) specific surface area of the synthetic  
115 acid birnessite was  $65 \pm 1 \text{ m}^2 \text{ g}^{-1}$ . The Average Oxidation State (AOS= 3.98 ( $\pm 0.02$ )) of synthetic  
116 birnessite was measured using the oxalic acid-permanganate back-titration method (more details  
117 are provided in the Supporting Information (SI)). Scanning Electron Microscope (SEM; JEOL  
118 JSM-7100F) and High-resolution Transmission Electron Microscope (HRTEM; JEOL 2100 LaB $_6$ )  
119 images showed a nanoflower-shaped birnessite consisting of nanoflakes aggregations (see Figures  
120 S2 and S3).

### 121 2.3. Adsorption/oxidation batch experiments

122 For all experiments, NaCl concentration was set to 10 mM. The pH was adjusted to the  
123 desired values using additions of 0.1M HCl or 0.1M NaOH solution and maintained constant  
124 throughout the experiments. Before experiments, acid birnessite was sonicated 5 min for better  
125 dispersion.

126 Batch experiments were carried out under ambient conditions. Solutions were spiked with  
127 aliquots of 1 mM PIP or BPA to achieve initial concentration of 20  $\mu\text{M}$ . An Aqueous suspension  
128 of acid birnessite (870  $\mu\text{M}$ ) was employed, and the effect of dissolved Mn(II) was investigated by  
129 adding small amounts of 0.05 M MnCl $_2$  solution. In the simultaneous experiments, PIP or BPA,  
130 acid birnessite and MnCl $_2$  solution were mixed at the same time. In the pre-equilibrium or  
131 sequential experiments, suspensions containing manganese oxides and MnCl $_2$  were stirred for a  
132 certain time (2 h or 24 h) before adding PIP. The agitation speed of the mixture was stirred at 300  
133 rpm during the experiments at room temperature. Aliquots of solution were periodically withdrawn

134 and filtered (0.2  $\mu\text{m}$ ) for compound analysis. Other aliquots without filtration were immediately  
135 mixed with NaOH or ascorbic acid to quench the reaction and release eventual sorbed compounds.  
136 The same procedure was applied to test the effect of Mn(II) in the presence of anions (silicate or  
137 phosphate) on PIP oxidation.

138 Mn(II)-birnessite isotherm experiments were performed at pH 4, 5.5, 7.5, 8 ( $\pm 0.1$ ) under  
139 oxic conditions. The experiments were employed in 50 mL polyethylene tubes at a total volume of  
140 50 mL solution using the same acid birnessite suspension density (870  $\mu\text{M}$ ) and initial aqueous  
141 Mn(II) concentrations in the range of 0 to 2000  $\mu\text{M}$ . The tubes were sealed by caps and then shaken  
142 continuously at 200 rpm. During the equilibration time, the pH was adjusted to maintain the initial  
143 value. After 2 days of equilibration, the samples were centrifuged for 30 min at 4500 rpm. The  
144 supernatants were filtered through 0.2  $\mu\text{m}$  membranes, while the centrifuged wet pastes of the acid  
145 birnessite obtained were analyzed by Attenuated Total Reflectance Fourier Transform Infrared  
146 Spectroscopy (ATR-FTIR) (more details are given in the SI). Mn(II) removal was calculated as  
147 the difference between the initial and final Mn(II) solution concentrations. To examine the impact  
148 of dissolved  $\text{O}_2$  on the Mn(II) sorption, parallel experiments with the same process at pH 4 and 5.5  
149 ( $\pm 0.1$ ) were conducted in glovebox under  $\text{N}_2$  atmosphere. All experiments were conducted in  
150 triplicates and the standard deviation was calculated for all experimental series.

#### 151 2.4. Analytical procedures

152 Aqueous concentrations of PIP or BPA were determined using High Performance Liquid  
153 Chromatography analysis with UV-vis detection (HPLC-UV) equipped with a reversed-phase C18  
154 column (250 mm  $\times$  4.6 mm i.d., 5  $\mu\text{m}$ ) and an UV-vis detector (Waters 2489). The mobile phase  
155 was a mixture of acetonitrile/water (15/85 v/v, PIP; 65/35 v/v, BPA) containing 0.1% formic acid.  
156 The flow rate of mobile phase was set at 0.5 mL/min (PIP) or 0.6 mL/min (BPA). The UV detector

157 was set to 278 nm for PIP and BPA. Silicate concentrations were determined by the molybdenum-  
158 blue colorimetric method.<sup>42</sup> Dissolved Mn(II) concentrations in supernatants were determined by  
159 Atomic Absorption Spectroscopy (AAS, AA140, Varian, Shimadzu). The byproducts of BPA and  
160 PIP oxidation were identified using Ultraperformance Liquid Chromatography-tandem Mass  
161 Spectrometry (UPLC-MS/MS) system. An electrospray interface was used for the MS  
162 measurements in positive ionisation mode and full scan acquisition. No quantification has been  
163 made by LC/MS because the identified byproducts are not commercially available. ATR-FTIR and  
164 XRD were performed to determine the possible transformation of solids upon Mn(II) sorption.  
165 More details of these analytical methods are given in the SI.

### 166 **3. Results and Discussion**

#### 167 **3.1. Removal kinetics of PIP and BPA with birnessite**

168 Kinetic batch experiments conducted at pH 5.5 showed complete removal of BPA within 1  
169 h of reaction time (Figure 1a). A delay in complete removal was observed when Mn(II) was added  
170 to MnO<sub>2</sub> suspension, *e.g.* 25 h was needed for complete removal with the highest Mn(II) loading  
171 (Mn(II)/MnO<sub>2</sub> = 0.23). Slower removal kinetics were observed for PIP when compared to BPA  
172 (Figure 1b). Mass balance showed that adsorption and oxidation are involved in the removal of  
173 BPA or PIP in presence of MnO<sub>2</sub> (Figures 1 and S5), even though the adsorption appears to be  
174 relatively low under our experimental conditions. The overall removal rate can be dominated by  
175 either the rate of intrinsic chemical reactions on the surface (adsorption following by oxidation) or  
176 the rate of diffusion of the solute to the surface.

177 Pseudo-first-order and pseudo-second-order models were used to describe the removal of  
178 BPA and PIP, respectively, after an extensive search for best-fitting kinetic models accounting for  
179 these experimental concentration profiles. The pseudo-first-order rate equation is given as:

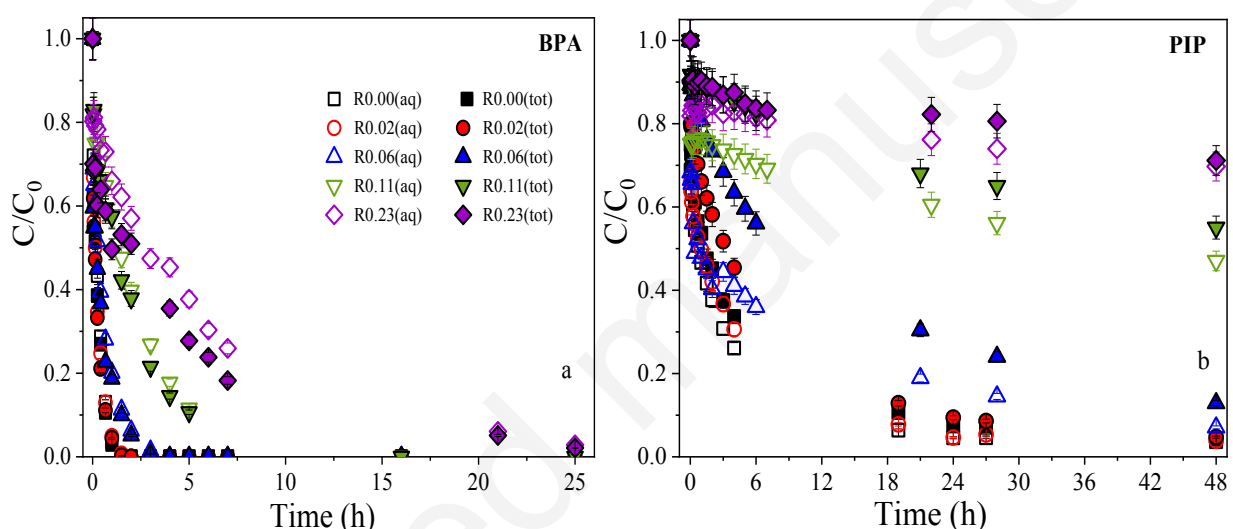
180 
$$\ln \frac{[BPA]_{tot}}{[BPA]_0} = -k_1 t \quad (1)$$

181 The pseudo-second-order equation is expressed as:

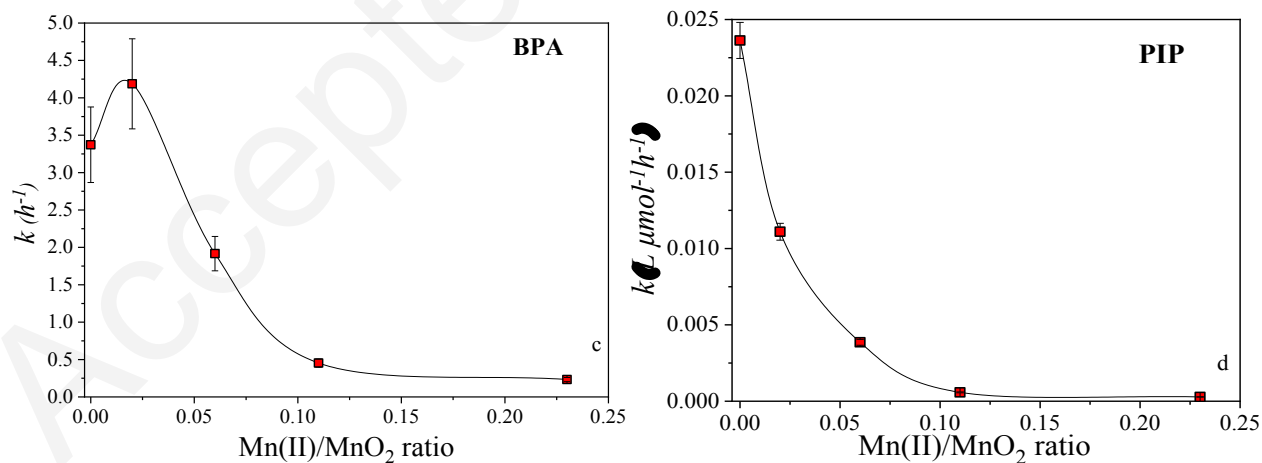
182 
$$\frac{1}{[PIP]_{tot}} = \frac{1}{[PIP]_0} + 2k_2 t \quad (2)$$

183 The pseudo-first-order apparent rate constant  $k_1$  ( $\text{h}^{-1}$ ) obtained by linear regression of  
184  $\ln([BPA]_{tot}/[BPA]_0)$  versus time were plotted against initial Mn(II) amount in Figure 1c. The  
185 pseudo-second-order rate constant,  $k_2$  ( $\text{L } \mu\text{mol}^{-1} \text{ h}^{-1}$ ), calculated from the slope of the plots of  
186  $1/[PIP]_{tot} - 1/[PIP]_0$  versus  $t$ , are given in Figure 1d (regression coefficients for all fitting is greater  
187 than 0.92). While a pseudo-first order may suppose no-chemical limiting step, the pseudo-second-  
188 order model suggests that the chemical reaction may be the rate-limiting step and the adsorption  
189 occurs probably via surface complexation reactions at specific sorption sites.<sup>43</sup> This falls in line  
190 with the PIP chemical structure where metal-bonded complexes with surface sites and/or directly  
191 hydrogen-bonded complexes with surface hydroxo groups involving both carboxylate and keto  
192 groups are expected based on previous investigations for analogous compounds.<sup>27, 44, 45</sup> At pH 5.5,  
193 PIP exists under zwitterionic form ( $\text{pK}_a$  5.20 and 6.38), whereas the BPA molecule is only in the  
194 protonated form (Figure S4). BPA containing only phenolic groups exhibits weaker sorption to  
195 metal surfaces through probably Van der Waals interactions and/or hydrogen bonds, but higher  
196 removal rate as compared to PIP (Figure 1). If the formation of the precursor complex is the rate-  
197 limiting step, our kinetic comparison let suppose that weaker binding of phenolic compounds are  
198 more energetically favorable than the surface complexation of polyfunctional carboxylated  
199 compounds. Afterwards, electron exchange of BPA with  $\text{MnO}_2$  form a radical, followed by a series  
200 of reactions including radical coupling, fragmentation, substitution and elimination to form  
201 multiple byproducts (up to 11 byproducts have been reported).<sup>20, 22, 24</sup> Our LC/MS analysis

202 identified one predominant species of mass-to-charge ratio of  $m/z=135$  as the most dominant  
 203 byproduct of BPA over the first reaction time (1 h), which likely corresponds to 4-hydroxycumy  
 204 alcohol according to previous investigation.<sup>46</sup> For PIP, LC/MS analysis confirmed the formation  
 205 of one predominant species of  $m/z=227$  (M-26) through N-dealkylation of the piperazine ring of  
 206 PIP. Indeed, the piperazine ring of PIP can be oxidized through two one-electron transfers from the  
 207 N atom of piperazine ring to Mn(IV), and then N-dealkylation and/or C-hydroxylation cause ring  
 208 opening, as typically observed for similar compounds.<sup>20,23,25</sup>



209



210

211

212

213

214 **Figure 1.** Top: Removal kinetics of BPA and PIP ( $(aq)$  = aqueous residual concentration;  $(tot)$  = total  
215 concentration representing both residual concentration and adsorbed concentration obtained after  
216 desorption. The R number refers to Mn(II)/MnO<sub>2</sub> ratio. Bottom: kinetic rate constants at different  
217 Mn(II)/MnO<sub>2</sub> ratio. Experimental conditions: [BPA or PIP] = 20  $\mu$ M; [acid birnessite] = 870  $\mu$ M; [NaCl]  
218 = 10 mM; pH = 5.5  $\pm$  0.1.

219 On the other hand, dissolved Mn(II) displayed suppressive effects on the removal rate of  
220 BPA and PIP (Figure 1). The rate constant for PIP sharply decreased with increasing in dissolved  
221 Mn(II) amount, whereas the rate constant for BPA did not significantly change between 0 and 50  
222  $\mu$ M (the difference is statistically not significant given the relative standard deviation, Figure 1)  
223 but later decreased with increasing in Mn(II) amount as for PIP. The decrease in the oxidative  
224 ability of MnO<sub>2</sub> in the presence of dissolved Mn(II) may result from competition of compound and  
225 Mn(II) to interact with reactive surface sites and/or aqueous complexation of compound with  
226 Mn(II). However, the effect of aqueous complexation reaction should be of less importance due to  
227 weaker binding (low stability constant) of phenols or quinolones with divalent cations such as  
228 Mn(II).<sup>47</sup> It should be noted that the PIP adsorbed amount at low Mn(II) loading first increased,  
229 probably due to favorable electrostatic interactions with MnO<sub>2</sub> surfaces because of the adsorption  
230 of Mn(II) ions, and then decreased over reaction time (Figure S5). On the other hand, strong  
231 binding of Mn(II) to MnO<sub>2</sub> surfaces suggests competition of target compounds and Mn(II) for  
232 surface sites. Indeed, complete removal of dissolved Mn(II) was observed for initial  $[Mn(II)]_{aq} <$   
233 100  $\mu$ M, whereas at the highest Mn(II) supplied amount (200  $\mu$ M) more than 60 % of Mn(II) was  
234 removed (Figure S6).

235 Previous studies have determined two different types of adsorption sites at the MnO<sub>6</sub>  
236 octahedra layers of layered type birnessite, 1) edge sites and 2) vacancy sites.<sup>48</sup> Edge sites are  
237 present on the edge of Mn octahedral sheets and are usually the first sites to react with

238 contaminants, whereas vacancy sites are present within the Mn octahedral sheets, and are typically  
239 associated with long-term adsorption and oxidation sites of contaminants through diffusion from  
240 the edge sites.<sup>13,25,49</sup> Previous reports<sup>25,50,51</sup> predicted that anionic compounds are likely to bind  
241 only at the edge sites of MnO<sub>2</sub>, whereas cationic Mn(II) could bind at both edge and vacancy sites.  
242 Wang et al.<sup>50</sup> reported that because of the highly negative charge of the vacancy sites, fulvic acid  
243 (negatively charged polycarboxylic compound) would bind preferentially to edges and not  
244 vacancies. Based on all these observations, we hypothesized that the total removal rate of PIP in  
245 our experimental scenario is controlled by the PIP adsorption onto surface sites (i.e. formation of  
246 the precursor complex) and/or the diffusion of Mn(II) from edge sites to vacancy sites, making the  
247 previously occupied edge sites available for further PIP binding. The latter diffusion process could  
248 explain the enhanced PIP adsorption during the initial kinetic phase, and subsequent oxidation of  
249 bound PIP as the reaction proceeded (Figure S5).

250 As an attempt to assess the time-dependent competition of PIP and Mn(II) towards MnO<sub>2</sub>  
251 surfaces, Mn(II) and MnO<sub>2</sub> (Mn(II)/MnO<sub>2</sub> ratio 0.11) were allowed for longer pre-equilibration  
252 times (2 h or 24 h pre-equilibration) before PIP addition instead of simultaneous mixing of all the  
253 three reactants. While the total removal rate of PIP is not significantly affected, the PIP adsorbed  
254 amount at the first kinetic stage decreased in pre-equilibrated tests, suggesting that adsorption sites  
255 for PIP may be pre-occupied with Mn(II) during the pre-equilibration period (Figure S7). When  
256 PIP and Mn(II) were reacted with MnO<sub>2</sub> at the same time, we speculate a competition between PIP  
257 and Mn(II) to bind at the edge sites of MnO<sub>2</sub> during the first kinetic phase. As a result, with  
258 increasing dissolved Mn(II) amounts, the competition for PIP binding to the edge sites also  
259 increases. Ultimately, the buildup of Mn(II) at the edge sites will continuously decrease PIP  
260 adsorption and the subsequent oxidation with time. A further kinetic modeling based on two types

261 of sorption sites (see details in the SI) confirmed that Mn(II) can alter both adsorption and oxidation  
262 reactions at MnO<sub>2</sub> surfaces. Taken together, our results showed that the amount of available  
263 dissolved Mn(II) considerably influenced organic contaminants interactions with MnO<sub>2</sub> surfaces.  
264 As pH may also affect Mn(II) redox reactions, the effect of pH on the PIP removal rate was  
265 investigated in the following section.

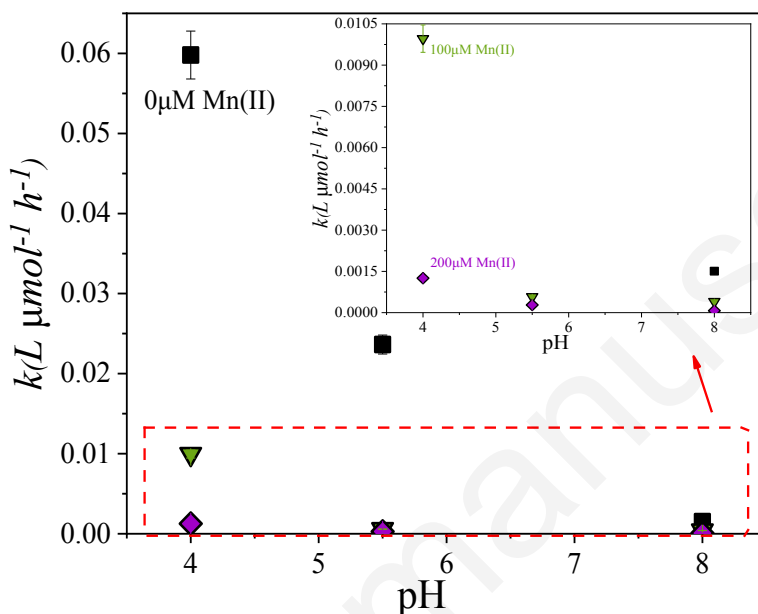
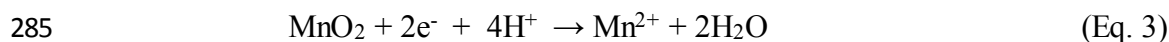
266

### 267 **3.2. Effects of pH and Mn(II) on the removal rate of PIP**

268 The removal kinetics of PIP at different initial concentrations of Mn(II) (0, 100, 200 μM) were  
269 compared at three pH values (4, 5.5 and 8). Figure 2 shows that pseudo-second-order rate constants  
270 of PIP removal were sensitive to solution pH. The rate constants for all investigated Mn(II)  
271 amounts (0, 100, and 200 μM) exhibited the same order, pH 4 > pH 5.5 > pH 8. This suggests that  
272 acidic conditions favored PIP removal, a trend also observed for analogous quinolones reacting  
273 with MnO<sub>2</sub>.<sup>23,52</sup> We attribute this to variability in two pH-dependent factors: 1) speciation of PIP  
274 that affects binding to MnO<sub>2</sub> surfaces and then oxidation (as described in section 3.1), and 2) redox-  
275 potential of MnO<sub>2</sub>.<sup>23,52</sup> PIP molecules were predominantly present in protonated (cationic),  
276 zwitterionic (neutral), and deprotonated (anionic) form at pH 4, 5.5, and 8 respectively (Figure S4).  
277 At relatively low pH, electrostatic interactions of positively charged PIP molecules are favored  
278 with the negatively charged surface of MnO<sub>2</sub> (PZC of MnO<sub>2</sub> is ~2.3-2.9).<sup>9,53</sup>

279 Increasing the pH enables more negative surface charge, thereby limiting the interactions with the  
280 negatively charged PIP.<sup>54</sup> We verified this experimentally as the amount of PIP adsorbed at pH 8  
281 was significantly less than that measured at pH 4 in all experiments (Figure S9). Second, a decrease  
282 in redox potential of MnO<sub>2</sub> from 0.99 V to 0.76 V has been reported when the pH increased from

283 4 to 8.<sup>55</sup> Indeed, reductive conversion of MnO<sub>2</sub> into Mn(II) is dependent on the amount of protons  
284 (Eq.3), which would result in increase in PIP removal rate when the pH decreases.

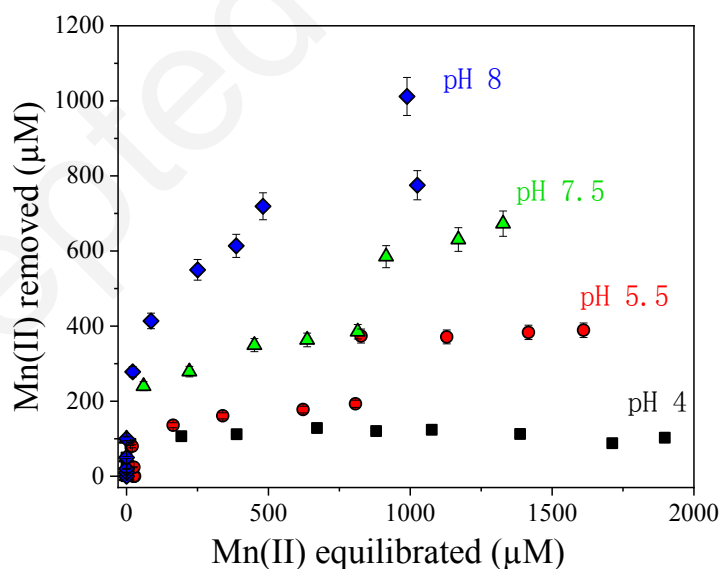


286  
287 **Figure 2.** Kinetic rate constants of PIP, plotted as a function of pH at different initial concentrations of  
288 Mn(II) (0, 100, 200 μM). Experimental conditions: [PIP] =20 μM; [acid birnessite] =870 μM; [NaCl] =10  
289 mM.

290 As expected, Mn(II) formed by reductive dissolution of MnO<sub>2</sub> was completely removed by  
291 binding to MnO<sub>2</sub> irrespective of the solution pH (Figure S9). Mn(II) was below AAS detection  
292 limit (<0.02 μM) in all experiments when no dissolved Mn(II) was supplied in the input solution  
293 (Figure S9). When dissolved Mn(II) was supplied, Mn(II) removal was, however, dependent on  
294 the pH value. Lower pH enabled more dissolved Mn(II), while more Mn(II) removal was observed  
295 at pH 8. For the highest Mn(II) amount (200 μM), the final steady-state Mn(II) concentrations  
296 were ~120 μM, ~75 μM, and ~20 μM at pH 4, 5.5, and 8 respectively. Similarly, dissolved Mn(II)  
297 was below the detection limit at both pH 5.5 and 8 when 100 μM Mn(II) was used, while a  
298 concentration of ~25 μM was still measured at pH 4.

299 As an attempt to check whether pH can influence the structure of acid birnessite under our  
300 experimental conditions, sorption isotherms coupled to ATR-FTIR experiments were investigated  
301 at a wide range of Mn(II) concentration (10-2000  $\mu\text{M}$ ). First, sorption isotherms showed different  
302 shape depending on pH value across the Mn(II) concentration range (Figure 3). Two stages of  
303 Mn(II) removal were observed at pH higher than 5.5, while at pH 4 a typical L-shape with a plateau  
304 was observed. Indeed, substantial increase in Mn(II) removal amount was observed at higher  
305 residual Mn(II) concentration and at pH higher than 5.5, following by either a plateau or continuous  
306 increase in removal amount. This S-shaped isotherm of dissolved Mn(II) adsorption by birnessite  
307 has been already reported in literature but only at pH higher than 7.<sup>31,32</sup> They have attributed this  
308 behavior to surface-catalyzed oxidation of Mn(II) by molecular oxygen enabling more Mn(II)  
309 sorption under oxic conditions relative to anoxic systems through the formation of low valence Mn  
310 oxides phases such as feitknechtite ( $\beta\text{-MnOOH}$ ) and/or manganite ( $\gamma\text{-MnOOH}$ ).

311



312

313 **Figure 3.** Mn(II) sorption isotherms at pH 4, 5.5, 7.5, 8  $\pm 0.1$  under oxic conditions. Experimental  
314 conditions: [acid birnessite] = 870  $\mu\text{M}$ ; [NaCl] = 10 mM; reaction time = 2 d.

315

316 To check whether this behavior may occur in our system at that pH range (i.e. lower than  
317 7), we conducted sorption isotherms under anoxic conditions at pH 4 and 5.5, and compared to  
318 those determined under ambient conditions. While at pH 4 the oxic and anoxic isotherms  
319 overlapped (data not shown), there was significant influence of oxygen on Mn(II) removal at pH  
320 5.5 (Figure S10). However, the ATR-FTIR spectra recorded for sample solids at pH 5.5 did not  
321 show any new Mn-phase over the Mn(II) concentration range (200 or 2000  $\mu\text{M}$ ) and equilibration  
322 time (2 d or 10 d) (Figure S11), probably due to the low formation extent of Mn<sup>III</sup>-bearing phase.  
323 Manganite was only detected at pH 8 and at high Mn(II) concentration (2000  $\mu\text{M}$ ), at 2 d of  
324 equilibration time (as for sorption isotherms) and at longer equilibration time (10 d) (Figure S11).  
325 Collectively, these results suggested no phase transformation under the experimental conditions  
326 used for kinetic assessment (e.g. 200  $\mu\text{M}$ ) over the investigated pH range. This was further  
327 confirmed by XRD analysis, where no notable transformation can be detected (Figure S12).

328 Despite no evident MnO<sub>2</sub> transformation, we cannot rule out the possibility of formation of  
329 Mn(III) species, via comproportionation reaction of adsorbed Mn(II) and structural Mn(IV) in  
330 birnessite especially at high pH.<sup>17,50,56</sup> It is well known that Mn(III) centers are an important surface  
331 features of birnessite and are involved in redox reactions with various organic compounds.<sup>29</sup> First,  
332 the average oxidation state of samples reacted with PIP only slightly decreased from 3.98 to 3.92  
333 ( $\pm 0.02$ ) over the investigated pH range. However, partial reduction of MnO<sub>2</sub> upon addition of 200  
334  $\mu\text{M}$  of dissolved Mn(II) dropped down the AOS to 3.68 ( $\pm 0.05$ ) at pH 4 and 5.5, and 3.52 ( $\pm 0.05$ )  
335 at pH 8. This decrease suggests that percentages of Mn(III) or Mn(II) or both are relatively higher  
336 after 48 h of reaction time with respect to the initial sample. The formation of Mn(III) after 48 h of  
337 reaction time in kinetic experiments was further confirmed by the detection of Mn(III)-  
338 pyrophosphate complex at 480 nm, Mn(III) being stabilized through ligand-binding complexes.<sup>57</sup>

339 As an attempt to check the mass balance of Mn(II), desorption tests with high amount of  
340 Ca(II) (25 mM) were conducted. This cation has been proposed as a desorption agent of solid  
341 bound Mn(II),<sup>58</sup> though adsorption of Ca(II) on vacant sites is much weaker than Mn(II).<sup>59</sup> It was  
342 also reported that Ca(II) may stabilize Mn(III) in the layers through stronger adsorption of Ca(II)  
343 in interlayer regions and then compensation of the charge deficiency caused by the presence of  
344 Mn(III).<sup>9,33,59</sup> More recently, Wang et al.,<sup>50</sup> reported that Ca(II) could exchange adsorbed Mn(II)  
345 from vacancy sites, but not block the edge sites. Then, Mn(II) may be oxidized preferentially on  
346 edge sites in presence of Ca(II) favoring Mn(III) production and potential formation of  
347 MnOOH/Mn<sub>3</sub>O<sub>4</sub> phases<sup>50</sup>. Mn(II) desorbed amounts were determined in PIP/MnO<sub>2</sub> suspensions  
348 subject or not to Mn(II) supplying and at different pH values (Figures S13 and S14). As expected  
349 in no-input Mn(II) experiments, more Mn(II) was desorbed at low pH values, as more PIP  
350 oxidation and more Mn(II) formation were observed at this pH range (Figure S13). However, the  
351 desorbed Mn(II) amount was still lower than the stoichiometric amount corresponding to the  
352 oxidized PIP (Figure S9). When 200 μM Mn(II) was present in the input solution, Ca(II) has almost  
353 no impact on the amount of dissolved Mn(II), yet a slight decrease in Mn(II) removal was observed  
354 at pH 4 and 5.5 (Figure S14). These results showed that Ca(II) failed to recover the removed  
355 Mn(II), thereby suggesting comproportionation reaction forming Mn(III), as previously reported in  
356 Wang et al.<sup>50</sup>.

357

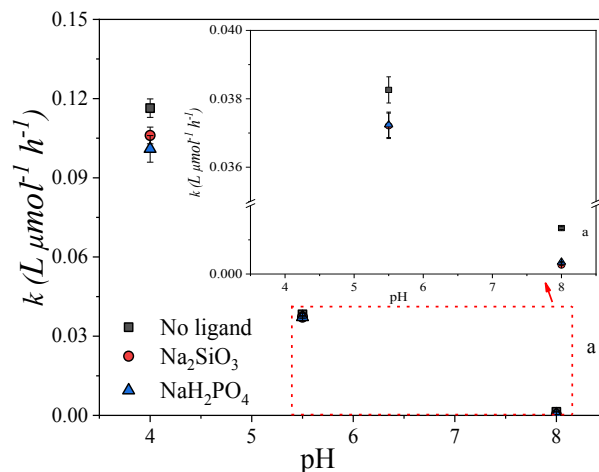
### 358 **3.3. Combined effects of Mn(II) and anions on the oxidation capacity of birnessite**

359 The effects of commonly found inorganic ligands, phosphate and silicate, on the oxidation of  
360 PIP with MnO<sub>2</sub> were investigated over the pH range (4-8). The two ligands exhibited similar effects  
361 on the PIP oxidation in presence or absence of dissolved Mn(II) (Figure 4). In no-input Mn(II)

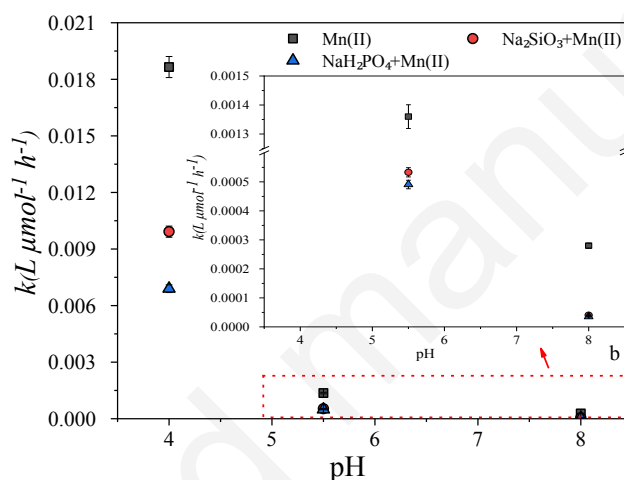
362 experiments, the presence of silicate or phosphate did not significantly influence the kinetic rate  
363 constants for PIP removal over the whole pH range, only a small decrease in all experiments was  
364 observed (Figure 4). However, when Mn(II) was added in the reaction medium, more than 2-times  
365 decrease in kinetic rate constants was measured at pH 4 and 5.5 in presence of silicate or phosphate,  
366 and much more (~10 times) at pH 8. It is worth noting that similar behavior was observed in the  
367 presence of another type of anion, 100  $\mu$ M of NaHCO<sub>3</sub> (pKa 6.3 and 10.5) at pH 8 (data not shown).  
368 Indeed, a significant effect on PIP oxidation was only observed in presence of Mn(II).

369 Sorption edges showed low affinity of silicate and phosphate (see speciation in Figure S16)  
370 to the negatively charged MnO<sub>2</sub> surfaces in absence of dissolved Mn(II). However, presence of  
371 Mn(II) relatively enhanced adsorption of silicate and phosphate into MnO<sub>2</sub> surfaces, particularly  
372 at high pH values (> 6) (Figure S17).

373



374



375 **Figure 4.** Kinetic rate constants of PIP vs pH in the absence or presence of silicate or phosphate: (a) no-  
 376 input Mn(II) experiments, (b)  $[\text{Mn(II)}]_0 = 100 \mu\text{M}$ . Experimental conditions:  $[\text{PIP}] = 20 \mu\text{M}$ ;  $[\text{acid birnessite}]$   
 377  $= 870 \mu\text{M}$ ;  $[\text{Na}_2\text{SiO}_3] = 100 \mu\text{M}$ ;  $[\text{NaH}_2\text{PO}_4] = 100 \mu\text{M}$ .

378

379 These results indicate that the pH-dependence of phosphate or silicate sorption is relatively  
 380 affected by the presence of Mn(II) ion, which may suppose an enhancement of adsorption of  
 381 anionic ligands through the formation of a surface-Mn(II)-ligand ternary complex. Indeed, Mn(II)  
 382 may act as a bridge ion to form a complex with the functional groups of ligand. The formation of  
 383 aqueous complexes of phosphate with Mn(II) ions has been previously reported and different  
 384 coordination modes have been proposed.<sup>60,61</sup> However, there is a lack of information about the  
 385 complexation of Mn(II) with dissolved silicate ions, but we may suppose that the aqueous

386 complexation of silicate with divalent cations such as Mn(II) is relatively weak, and lower than  
387 that with phosphate.<sup>62</sup> Furthermore, according to the Irving-Williams series<sup>63</sup> and cation adsorption  
388 data<sup>55</sup> ternary surface complexation of cations such as Mn(II), Co(II) and Ni(II) with silicate are  
389 supposed to follow the order: Mn(II) < Co(II) < Ni(II). As a result, the stability constant value of  
390 Mn(II) should be lower than that previously determined for Ni(II), Ni(OSi(OH)<sub>3</sub>)<sup>+</sup>, log β= 6.34 at  
391 I= 0.00M.<sup>64</sup> Because both ligands exhibited similar effects on removal kinetics, there are probably  
392 additional factors which may explain enhanced suppressive effects in presence of these ligands.

393 As dissolved Mn(II) was completely removed from solution at pH 5.5 and 8 over the first  
394 reaction time, enhancement in Mn(II) removal due to the presence of anions cannot be highlighted.  
395 At pH 4, no significant change in Mn(II) removal has been observed upon addition of ligands. On  
396 the other hand, possible formation of precipitates (*e.g.* phosphate or carbonate with manganese  
397 ions) is not expected under our experimental conditions due to the low degree of saturation. Indeed,  
398 the lower aqueous concentration of free Mn(II) (particularly after adsorption) or ligand exclude a  
399 possibility of such precipitation based on the mineral solubility, *i.e.* according to the solubility  
400 constant of Mn(II) phosphate (log K<sub>s</sub> = - 27.07)<sup>65</sup> and MnCO<sub>3</sub> (log K<sub>s</sub> = - 10.58).<sup>66</sup> In addition,  
401 FTIR analysis of reacted samples did not reveal any new precipitate (data not shown).

402 While interactions of silicate with MnO<sub>2</sub> is rarely investigated, adsorption of phosphate has  
403 been described by the formation of outer-sphere complexes with surface hydroxyl groups of δ-  
404 MnO<sub>2</sub> at the same pH range (4-8).<sup>14,67</sup> On the other hand, potential change of the surface charge  
405 from negative to positive by exchange of H<sup>+</sup> on the MnO<sub>2</sub> surface may occur during Mn(II)  
406 adsorption, a phenomenon also observed during the adsorption of arsenate in presence of Ca(II) or  
407 Mg(II).<sup>14,67</sup> The Mn(II) adsorption should lead to a decrease in the negative surface charge, thereby  
408 enhancing ability to bind anions and ultimately competition with target compounds. Therefore,

409 positively charged MnO<sub>2</sub> surface may favor adsorption of anionic compounds like phosphate and  
410 silicate through electrostatic attraction. Indeed, in experiments with input Mn(II), competition  
411 between PIP and silicate/phosphate to bind at the MnO<sub>2</sub> edge sites can be responsible for  
412 suppressed PIP oxidation. However, in experiments with no input Mn(II), potential changes in  
413 surface charge of MnO<sub>2</sub> caused by the *in situ* generated Mn(II) was probably not sufficient to  
414 permit favorable electrostatic binding of silicate/phosphate. Hence, negligible influence in PIP  
415 adsorption and removal rates has been observed in this setup. Furthermore, possible stabilization  
416 of dissolved Mn(III) through ligand complexation with phosphate or silicate (as generally reported  
417 for pyrophosphate) cannot be verified because of the lack of data on complexation reactions.  
418 Nevertheless, this potential stabilization of Mn(III) could be excluded because no significant  
419 impact of phosphate or silicate has been observed in no-input Mn(II) experiments. Overall, the  
420 results suggest that the MnO<sub>2</sub>-bound Mn(II) system could adsorb more effectively anions such as  
421 phosphate or silicate and thus reducing interactions with organic compounds.<sup>56</sup>

#### 422 **4. Conclusions**

423 We have notably demonstrated that dissolved Mn(II) and anionic ligands, commonly found  
424 in terrestrial and aquatic environments, concurrently affect the adsorption and oxidation of organic  
425 compounds on nanostructured MnO<sub>2</sub> surfaces. In contrast to phenolic compounds where adsorption  
426 is mainly driven by weak van der Waals-type hydrophobic interactions, removal kinetics of  
427 carboxylated compounds (e.g. PIP) generally bound to MnO<sub>2</sub> through surface complexation  
428 reactions exhibited two-stage behavior. During the initial kinetic stage, there was competition  
429 between compound and Mn(II) for binding at edge sites, while accumulation of Mn(II) at both  
430 edge and vacancy sites continuously decreased adsorption and subsequent oxidation over time.  
431 Furthermore, pH affected redox interactions of Mn(II) on MnO<sub>2</sub> surfaces and Mn(II)-Mn(IV)

432 comproportionation reaction, thus decreasing adsorption and oxidation processes. Nanostructured  
433 birnessite, with a surface charge modified upon Mn(II) binding, adsorbed more effectively anionic  
434 ligands such as phosphate or silicate and thus reducing interactions with organic compounds at a  
435 range of environmentally relevant pH values. Therefore, co-existing anions and dissolved Mn(II)  
436 must be considered when examining the reactivity of nanostructured birnessite under  
437 environmentally relevant conditions. These findings call for consideration of the co-binding effects  
438 of cations and anions on the surface charge of birnessite-type manganese oxide nanoparticles, in  
439 contaminant fate and transport modeling studies.

440

#### 441 **Conflicts of interest**

442 There are no conflicts to declare.

443

#### 444 **Acknowledgements**

445 This work was supported by the Institut Universitaire de France (IUF) and Région Bretagne (SAD).

446 We gratefully acknowledge the Chinese Scholarship Council of PR China for providing financial

447 support for Qinzhi Li to stay at the ENSCR. We are also thankful to Sylvain Giraudet (BET),

448 Valerie Courousse (AAS), Isabelle Soutrel (LC/MS), Francis Gouttefangeas (ScanMAT, SEM)

449 and Vincent Dorcet (ScanMAT, TEM) for their assistance.

#### 450 **Footnote**

451 † Electronic supplementary information (ESI) associated with this article can be found in the online

452 version: Additional information regarding analytical and characterization techniques, SEM/TEM

453 images, additional data on removal kinetics and kinetic modeling, ATR-FTIR and XRD data,

454 anions adsorption and speciation.

455

456 **References**

- 457 1 J. E. Post, Manganese oxide minerals: Crystal structures and economic and environmental  
458 significance, *Proc. Natl. Acad. Sci*, 1999, **96**, 3447-3454.
- 459 2 D. R. Learman, B. M. Voelker, A. I. Vazquez-Rodriguez and C. M. Hansel, Formation of  
460 manganese oxides by bacterially generated superoxide, *Nat. Geosci*, 2011, **4**, 95-98.
- 461 3 M. Villalobos, B. Lanson, A. Manceau, B. Toner and G. Sposito, Structural model for the  
462 biogenic Mn oxide produced by *Pseudomonas putida*, *Am. Mineral*, 2006, **91**, 489-502.
- 463 4 S. M. Webb, B. M. Tebo and J. R. Bargar, Structural characterization of biogenic Mn oxides  
464 produced in seawater by the marine bacillus sp. strain SG-1, *Am. Mineral*, 2005, **90**, 1342-  
465 1357.
- 466 5 H. Zhao, M. Zhu, M. W. Li, E. J. Elzinga, M. Villalobos, F. Liu, J. Zhang, X. Feng and D. L.  
467 Sparks, Redox Reactions between Mn(II) and Hexagonal Birnessite Change Its Layer  
468 Symmetry, *Environ. Sci. Technol*, 2016, **50**, 1750-1758.
- 469 6 J. R. Bargar, B. M. Tebo, U. Bergmann, S. M. Webb, P. Glatzel, V. Q. Chiu and M. Villalobos,  
470 Biotic and abiotic products of Mn(II) oxidation by spores of the marine *Bacillus* sp. strain SG-  
471 1, *Am. Mineral*, 2005, **90**, 143-154.
- 472 7 Z. Wu, C. L. Peacock, B. Lanson, H. Yin, L. Zheng, Z. Chen, W. Tan, G. Qiu, F. Liu and X.  
473 Feng, Transformation of Co-containing birnessite to todorokite: effect of Co on the  
474 transformation and implications for Co mobility, *Geochim. Cosmochim. Acta*, 2019, **246**, 21-  
475 40.
- 476 8 V. A. Drits, B. Lanson and A.-C. Gaillot, Birnessite polytype systematics and identification by  
477 powder X-ray diffraction, *Am. Mineral*, 2007, **92**, 771-788.

- 478 9 C. L. Peacock and D. M. Sherman, Sorption of Ni by birnessite: Equilibrium controls on Ni in  
479 seawater, *Chem. Geol*, 2007, **238**, 94-106.
- 480 10 B. M. Tebo, J. R. Bargar, B. G. Clement, G. J. Dick, K. J. Murray, D. Parker, R. Verity and S.  
481 M. Webb, Biogenic manganese oxides: Properties and mechanisms of formation, *Ann. Rev.*  
482 *Earth. Planet. Sci*, 2004, **32**, 287-328.
- 483 11 N. Birkner and A. Navrotsky, Thermodynamics of manganese oxides: Sodium, potassium, and  
484 calcium birnessite and cryptomelane, *Proc. Natl. Acad. Sci*, 2017, **114**, E1046-E1053.
- 485 12 J. G. Holguera, I. D. Etui, L. H. S. Jensen and J. Peña, Contaminant loading and competitive  
486 access of Pb, Zn and Mn(III) to vacancy sites in biogenic MnO<sub>2</sub>, *Chem. Geol*, 2018, **502**, 76-  
487 87.
- 488 13 M. Villalobos, In *Advances in the Environmental Biogeochemistry of Manganese Oxides*,  
489 American Chemical Society, 2015, Vol. 1197, ch. 4, pp. 65-87, DOI: 10.1021/bk-2015-  
490 1197.ch004.
- 491 14 W. Yao and F. J. Millero, Adsorption of Phosphate on Manganese Dioxide in Seawater,  
492 *Environ. Sci. Technol*, 1996, **30**, 536-541.
- 493 15 K. Saeki, S. Matsumoto and R. Tatsukawa, Selenite adsorption by manganese oxides, *Soil. Sci*,  
494 1995, **160**, 265-272.
- 495 16 C. Tournassat, L. Charlet, D. Bosbach and A. Manceau, Arsenic(III) Oxidation by Birnessite  
496 and Precipitation of Manganese(II) Arsenate, *Environ. Sci. Technol*, 2002, **36**, 493-500.
- 497 17 B. J. Lafferty, M. Ginder-Vogel and D. L. Sparks, Arsenite Oxidation by a Poorly Crystalline  
498 Manganese-Oxide 1. Stirred-Flow Experiments, *Environ. Sci. Technol*, 2010, **44**, 8460-8466.

- 499 18 E. Lemarchand, J. Schott and J. Gaillardet, How surface complexes impact boron isotope  
500 fractionation: Evidence from Fe and Mn oxides sorption experiments, *Earth. Planet. Sci. Lett.*,  
501 2007, **260**, 277-296.
- 502 19 H. Peng, I. G. McKendry, R. Ding, A. C. Thenuwara, Q. Kang, S. L. Shumlas, D. R. Strongin,  
503 M. J. Zdilla and J. P. Perdew, Redox properties of birnessite from a defect perspective, *Proc.*  
504 *Natl. Acad. Sci. U.S.A.*, 2017, **114**, 9523-9528.
- 505 20 C. K. Remucal and M. Ginder-Vogel, A critical review of the reactivity of manganese oxides  
506 with organic contaminants, *Environ. Sci. Pro. Impacts*, 2014, **16**, 1247-1266.
- 507 21 W. T. Jiang, P. H. Chang, Y. S. Wang, Y. Tsai, J. S. Jean, Z. Li and K. Krukowski, Removal  
508 of ciprofloxacin from water by birnessite, *J. Hazard. Mater.*, 2013, **250-251**, 362-369.
- 509 22 S. Balgooyen, P. J. Alaimo, C. K. Remucal and M. Ginder-Vogel, Structural Transformation  
510 of MnO<sub>2</sub> during the Oxidation of Bisphenol A, *Environ. Sci. Technol*, 2017, **51**, 6053-6062.
- 511 23 H. Zhang and C. H. Huang, Oxidative Transformation of Fluoroquinolone Antibacterial Agents  
512 and Structurally Related Amines by Manganese Oxide, *Environ. Sci. Technol*, 2005, **39**, 4474-  
513 4483.
- 514 24 K. Lin, W. Liu and J. Gan, Oxidative removal of bisphenol A by manganese dioxide: efficacy,  
515 products, and pathways, *Environ. Sci. Technol*, 2009, **43**, 3860-3864.
- 516 25 R. Pokharel, Q. Li, L. Zhou and K. Hanna, Water flow and dissolved MnII alter transformation  
517 of pipemidic acid by manganese oxide, *Environ. Sci. Technol*, 2020, **54**, 8051-8060.
- 518 26 B. J. Lafferty, M. Ginder-Vogel, M. Zhu, K. J. T. Livi and D. L. Sparks, Arsenite Oxidation  
519 by a Poorly Crystalline Manganese-Oxide. 2. Results from X-ray Absorption Spectroscopy  
520 and X-ray Diffraction, *Environ. Sci. Technol*, 2010, **44**, 8467-8472.

- 521 27 M. Kamagate, M. Pasturel, M. Brigante and K. Hanna, Mineralization Enhancement of  
522 Pharmaceutical Contaminants by Radical-Based Oxidation Promoted by Oxide-Bound Metal  
523 Ions, *Environ. Sci. Technol*, 2020, **54**, 476-485.
- 524 28 S. Balgooyen, G. Campagnola, C. K. Remucal and M. Ginder-Vogel, Impact of bisphenol A  
525 influent concentration and reaction time on MnO<sub>2</sub> transformation in a stirred flow reactor,  
526 *Environ. Sci. Proc. Impacts*, 2019, **21**, 19-27.
- 527 29 P. S. Nico and R. J. Zasoski, Mn(III) center availability as a rate controlling factor in the  
528 oxidation of phenol and sulfide on  $\delta$ -MnO<sub>2</sub>, *Environ. Sci. Technol*, 2001, **35**, 3338-3343.
- 529 30 J. Huang, S. Zhong, Y. Dai, C.-C. Liu and H. Zhang, Effect of MnO<sub>2</sub> Phase Structure on the  
530 Oxidative Reactivity toward Bisphenol A Degradation, *Environ. Sci. Technol*, 2018, **52**,  
531 11309-11318.
- 532 31 J. P. Lefkowitz, A. A. Rouff and E. J. Elzinga, Influence of pH on the Reductive Transformation  
533 of Birnessite by Aqueous Mn (II), *Environ. Sci. Technol*, 2013, **47**, 10364-10371.
- 534 32 E. J. Elzinga, Reductive Transformation of Birnessite by Aqueous Mn(II), *Environ. Sci.*  
535 *Technol*, 2011, **45**, 6366-6372.
- 536 33 P. Yang, J. E. Post, Q. Wang, W. Xu, R. Geiss, P. R. McCurdy and M. Zhu, Metal adsorption  
537 controls the stability of layered manganese oxides, *Environ. Sci. Technol*, 2019, **53**, 7453-  
538 7462.
- 539 34 P. Yang, S. Lee, J. E. Post, H. Xu, Q. Wang, W. Xu and M. Zhu, Trivalent manganese on  
540 vacancies triggers rapid transformation of layered to tunneled manganese oxides (TMOs):  
541 Implications for occurrence of TMOs in low-temperature environment, *Geochim. Cosmochim.*  
542 *Acta*, 2018, **240**, 173-190.

- 543 35 A. Piazza, L. C. Casalini L, V. A. Pacini, G. Sanguinetti, J. Ottado and N. Gottig, Environmental  
544 bacteria involved in manganese (II) oxidation and removal from groundwater, *Front.*  
545 *Microbiol*, 2019, **10**, 119.
- 546 36 A. M. Gounot, Microbial oxidation and reduction of manganese: consequences in groundwater  
547 and applications, *FEMS Microbiol. Rev*, 1994, **14**, 339-349.
- 548 37 A. Careghini, A. F. Mastorgio, S. Saponaro and E. Sezenna, Bisphenol A, nonylphenols,  
549 benzophenones, and benzotriazoles in soils, groundwater, surface water, sediments, and food:  
550 a review, *Environ. Sci. Pollut. Res. Int*, 2015, **22**, 5711-5741.
- 551 38 M. Boy-Roura, J. Mas-Pla, M. Petrovic, M. Gros, D. Soler, D. Brusi and A. Mencio, Towards  
552 the understanding of antibiotic occurrence and transport in groundwater: Findings from the  
553 Baix Fluvià alluvial aquifer (NE Catalonia, Spain), *Sci. Total Environ*, 2018, **612**, 1387-1406.
- 554 39 G. Ding, G. Chen, Y. Liu, M. Li and X. Liu, Occurrence and risk assessment of fluoroquinolone  
555 antibiotics in reclaimed water and receiving groundwater with different replenishment  
556 pathways, *Sci. Total Environ*, 2020, **738**, 139802.
- 557 40 S. Xie, S. Manuguri, G. Proietti, J. Romson, Y. Fu, A. K. Inge, B. Wu, Y. Zhang, D. Häll, O.  
558 Ramström and M. Yan, Design and synthesis of theranostic antibiotic nanodrugs that display  
559 enhanced antibacterial activity and luminescence, *Proc. Natl. Acad. Sci. U.S.A.*, 2017, **114**,  
560 8464-8469.
- 561 41 R. McKenzie, The synthesis of birnessite, cryptomelane, and some other oxides and hydroxides  
562 of manganese, *Mineral. Mag*, 1971, **38**, 493-502.
- 563 42 J. Mullin and J. Riley, The colorimetric determination of silicate with special reference to sea  
564 and natural waters, *Anal. Chim. Acta*, 1955, **12**, 162-176.

- 565 43 Y. S. Ho and G. McKay, A comparison of chemisorption kinetic models applied to pollutant  
566 removal on various sorbents, *Process. Saf. Environ. Prot.*, 1998, **76**, 332-340.
- 567 44 L. Zhou, S. Martin, W. Cheng, L. Lassabatere, J.-F. Boily and K. Hanna, Water flow variability  
568 affects adsorption and oxidation of ciprofloxacin onto hematite, *Environ. Sci. Technol.*, 2019,  
569 **53**, 10102-10109.
- 570 45 S. Martin, A. Shchukarev, K. Hanna and J.-F. Boily, Kinetics and Mechanisms of Ciprofloxacin  
571 Oxidation on Hematite Surfaces, *Environ. Sci. Technol.*, 2015, **49**, 12197-12205.
- 572 46 J. Im, C. W. Prevatte, S. R. Campagna and F. E. Löffler, Identification of 4-Hydroxycumyl  
573 Alcohol As the Major MnO<sub>2</sub>-Mediated Bisphenol A Transformation Product and Evaluation  
574 of Its Environmental Fate, *Environ. Sci. Technol.*, 2015, **49**, 6214-6221.
- 575 47 A. Cuprys, R. Pulicharla, S. K. Brar, P. Drogui, M. Verma and R. Y. Surampalli,  
576 Fluoroquinolones metal complexation and its environmental impacts, *Coord. Chem. Rev.*,  
577 2018, **376**, 46-61.
- 578 48 V. A. Drits, E. Silvester, A. I. Gorshkov and A. Manceau, Structure of synthetic monoclinic  
579 Na-rich birnessite and hexagonal birnessite: I. Results from X-ray diffraction and selected-  
580 area electron diffraction, *Am. Mineral.*, 1997, **82**, 946.
- 581 49 Y. Wang, S. Benkaddour, F. F. Marafatto and J. Peña, Diffusion- and pH-dependent reactivity  
582 of layer-type MnO<sub>2</sub>: Reactions at particle edges versus vacancy sites, *Environ. Sci. Technol.*,  
583 2018, **52**, 3476-3485.
- 584 50 Q. Wang, P. Yang and M. Zhu, Effects of metal cations on coupled birnessite structural  
585 transformation and natural organic matter adsorption and oxidation, *Geochim. Cosmochim.*  
586 *Acta*, 2019, **250**, 292-310.

- 587 51 M. Villalobos, I. N. Escobar-Quiroz and C. Salazar-Camacho, The influence of particle size  
588 and structure on the sorption and oxidation behavior of birnessite: I. Adsorption of As (V) and  
589 oxidation of As (III), *Geochim. Cosmochim. Acta*, 2014, **125**, 564-581.
- 590 52 H. Zhang, W. R. Chen and C. H. Huang, Kinetic Modeling of Oxidation of Antibacterial Agents  
591 by Manganese Oxide, *Environ. Sci. Technol*, 2008, **42**, 5548-5554.
- 592 53 J. G. Catts and D. Langmuir, Adsorption of Cu, Pb and Zn by  $\delta\text{MnO}_2$ : Applicability of the site  
593 binding-surface complexation model, *Appl. Geochemistry*, 1986, **1**, 255-264.
- 594 54 L. Xu, C. Xu, M. Zhao, Y. Qiu and G. D. Sheng, Oxidative removal of aqueous steroid estrogens  
595 by manganese oxides, *Water. Res*, 2008, **42**, 5038-5044.
- 596 55 W. Stumm and J. J. Morgan, In *Aquatic chemistry: chemical equilibria and rates in natural*  
597 *waters*, John Wiley & Sons, 2012, Vol.126.
- 598 56 Q. Wang, P. Yang and M. Zhu, Structural transformation of birnessite by fulvic acid under  
599 anoxic conditions, *Environ. Sci. Technol*, 2018, **52**, 1844-1853.
- 600 57 S. M. Webb, G. J. Dick, J. R. Bargar and B. M. Tebo, Evidence for the presence of Mn (III)  
601 intermediates in the bacterial oxidation of Mn (II), *Proc. Natl. Acad. Sci*, 2005, **102**, 5558-  
602 5563.
- 603 58 B. J. Lafferty, M. Ginder-Vogel and D. L. Sparks, Arsenite oxidation by a poorly-crystalline  
604 manganese oxide. 3. Arsenic and manganese desorption, *Environ. Sci. Technol*, 2011, **45**,  
605 9218-9223.
- 606 59 M. Zhu, M. Ginder-Vogel, S. J. Parikh, X.-H. Feng and D. L. Sparks, Cation effects on the  
607 layer structure of biogenic Mn-oxides, *Environ. Sci. Technol*, 2010, **44**, 4465-4471.
- 608 60 C. K. Sharma, C. C. Chusuei, R. Clérac, T. Möller, K. R. Dunbar and A. Clearfield, Magnetic  
609 property studies of manganese-phosphate complexes, *Inorg. Chem*, 2003, **42**, 8300-8308.

- 610 61 S. Heintze, Manganese-phosphate reactions in aqueous systems and the effects of applications  
611 of monocalcium phosphate, on the availability of manganese to oats in an alkaline fen soil,  
612 *Plant. Soil*, 1968, **29**, 407-423.
- 613 62 R. H. Byrne, J. H. Lee and L. S. Bingler, Rare earth element complexation by  $\text{PO}_4^{3-}$  ions in  
614 aqueous solution, *Geochim. Cosmochim. Acta*, 1991, **55**, 2729-2735.
- 615 63 H. Irving and R. Williams, 637. The stability of transition-metal complexes, *J. Chem. Soc.*  
616 *(Resumed)*, 1953, 3192-3210.
- 617 64 P. N. Pathak and G. R. Choppin, Complexation/speciation studies of  $\text{Ni}^{2+}$  ion with ortho silicic  
618 acid in perchlorate media, *J. Radioanal. Nucl. Chem*, 2006, **267**, 309-314.
- 619 65 G. Friedl, B. Wehrli and A. Manceau, Solid phases in the cycling of manganese in eutrophic  
620 lakes: New insights from EXAFS spectroscopy, *Geochim. Cosmochim. Acta*, 1997, **61**, 275-  
621 290.
- 622 66 K. S. Johnson, Solubility of rhodochrosite ( $\text{MnCO}_3$ ) in water and seawater, *Geochim.*  
623 *Cosmochim. Acta*, 1982, **46**, 1805-1809.
- 624 67 T. Takamatsu, M. Kawashima and M. Koyama, The role of  $\text{Mn}^{2+}$ -rich hydrous manganese  
625 oxide in the accumulation of arsenic in lake sediments, *Water. Res*, 1985, **19**, 1029-1032.
- 626